SLEEPJ, 2020, 1–16

doi: 10.1093/sleep/zsaa108
Advance Access Publication Date: 1 June 2020
Original Article

ORIGINAL ARTICLE

Homeostatic state of microglia in a rat model of chronic sleep restriction

Shannon Hall[1], Samüel Deurveilher[1], George S. Robertson[2,3] and Kazue Semba[1,3,4,*]

[1]Department of Medical Neuroscience, Dalhousie University, Halifax, NS, Canada, [2]Department of Pharmacology, Dalhousie University, Halifax, NS, Canada, [3]Department of Psychiatry, Dalhousie University, Halifax, NS, Canada and [4]Department of Psychology & Neuroscience, Dalhousie University, Halifax, NS, Canada

*Corresponding author. Kazue Semba, Department of Medical Neuroscience, Dalhousie University, 5850 College Street, PO Box 15000, Halifax, Nova Scotia B3H 4R2, Canada. Email: k.semba@dal.ca.

Abstract

Chronic sleep restriction (CSR) negatively impacts brain functions. Whether microglia, the brain's resident immune cells, play any role is unknown. We studied microglia responses to CSR using a rat model featuring slowly rotating wheels (3 h on/1 h off), which was previously shown to induce both homeostatic and adaptive responses in sleep and attention. Adult male rats were sleep restricted for 27 or 99 h. Control rats were housed in locked wheels. After 27 and/or 99 h of CSR, the number of cells immunoreactive for the microglia marker ionized calcium-binding adaptor molecule-1 (Iba1) and the density of Iba1 immunoreactivity were increased in 4/10 brain regions involved in sleep/wake regulation and cognition, including the prelimbic cortex, central amygdala, perifornical lateral hypothalamic area, and dorsal raphe nucleus. CSR neither induced mitosis in microglia (assessed with bromodeoxyuridine) nor impaired blood–brain barrier permeability (assessed with Evans Blue). Microglia appeared ramified in all treatment groups and, when examined quantitatively in the prelimbic cortex, their morphology was not affected by CSR. After 27 h, but not 99 h, of CSR, mRNA levels of the anti-inflammatory cytokine interleukin-10 were increased in the frontal cortex. Pro-inflammatory cytokine mRNA levels (tumor necrosis factor-α, interleukin-1β, and interleukin-6) were unchanged. Furthermore, cortical microglia were not immunoreactive for several pro- and anti-inflammatory markers tested, but were immunoreactive for the purinergic P2Y12 receptor. These results suggest that microglia respond to CSR while remaining in a physiological state and may contribute to the previously reported homeostatic and adaptive responses to CSR.

Statement of Significance

Chronic sleep restriction is common in our society and alters sleep homeostasis with serious impacts on performance and health. Using a rat model of chronic sleep restriction, we show that microglia (immune cells in the brain) may be involved in these consequences of chronic sleep loss. The microglial marker Iba1 increased in brain regions involved in sleep/wake regulation and cognition, but without signs of inflammatory activation. These non-inflammatory responses of microglia may be part of the mechanisms leading to altered sleep regulation and cognitive impairments following insufficient sleep. Understanding the processes by which chronic sleep restriction impacts microglia and determining whether chronic sleep loss alters how microglia react to subsequent immunological challenges remain topics for future research.

Key words: sleep deprivation; Iba1; P2Y12 receptor; inflammatory markers; cytokines; immunohistochemistry; qRT-PCR

Submitted: 18 January, 2020; **Revised:** 13 May, 2020

Introduction

Chronic sleep restriction (CSR), characterized by habitual sleep insufficiency, is common in today's "24/7" society and negatively impacts cognition, mood, and health [1–3]. Rodent models of CSR have shown that CSR affects brain function at both cellular and molecular levels, impairing neuronal functions, and even causing neuronal loss [4]. Microglia play an important role in brain function in both health and disease [5], and it is possible that these innate immune cells, in addition to neurons and other glial cells, are involved in the physiological and cognitive responses to CSR.

Microglia are the resident macrophages of the central nervous system and play an essential role in mediating inflammation and promoting tissue repair [6] as well as in synaptic plasticity [7, 8]. There is growing evidence that microglia are involved in sleep regulation [3, 9]. Microglia activation after sleep loss has been reported in brain areas associated with cognitive functions [10–16]. For example, microglia increased in number and displayed larger cell bodies with thickened processes in the rat hippocampus after 5 days of sleep fragmentation [11]. In addition, following 4.5 days of CSR, microglia adopted a less ramified morphology suggestive of immunological activation and were detected phagocytosing presynaptic terminals in the adolescent mouse cortex [10]. Whether CSR activates microglia in brain regions that regulate sleep/wake cycles is unknown.

We previously developed and validated a rat model of CSR that takes into account the polyphasic sleep patterns of this species. In this model, alternating cycles of 3 h of sleep deprivation and 1 h of sleep opportunity, using programmable activity wheels that rotate slowly, are imposed over 4 or 6 days, to keep rats intermittently awake [17, 18]. This "3/1" protocol was effective in reducing both non-rapid eye movement (NREM) and rapid eye movement (REM) sleep amounts by approximately 60% from baseline levels. It induced homeostatic responses (rebound increases in NREM and REM sleep amounts and NREM sleep intensity during the sleep opportunities over the 4-day period) in conjunction with adaptive changes (gradual decline in NREM sleep intensity rebound during the sleep opportunities over 4 days, and limited sleep recovery after the 4-day CSR protocol [17]). These sleep responses to CSR were paralleled by impairment followed by a partial recovery in the performance on a sustained attention task during the same CSR protocol [18]. At the cellular level, the 3/1 protocol resulted in increased levels of brain-derived neurotrophic factor (BDNF) [19], which is involved in neuroprotection and synaptic plasticity [20, 21] as well as sleep intensity and sleep need [22, 23], and FosB family proteins [24], which are transcription factors indicating chronic neuronal activation [25], in a number of brain areas involved in sleep/wake regulation and cognitive functions.

In the present study, we investigated microglia responses to 4 days of the 3/1 CSR protocol in sleep/wake, limbic, and autonomic regions in the rat brain. We used immunohistochemistry for the well-established microglia/macrophage-specific marker ionized calcium-binding adaptor molecule-1 (Iba1), pro- and anti-inflammatory molecular markers of microglia activation [26], and the purinergic P2Y12 receptor marker of physiological or "homeostatic" microglia [27, 28], as well as assays for inflammatory cytokine expression.

Methods

Animals

Adult male Wistar rats (n = 90; Charles River Canada, St. Constant, QC), 300–350 g on arrival, were initially housed in pairs in a colony room under a 12 h:12 h light:dark cycle (lights on at 07:00 am) at 23 ± 1°C, with food and water available ad libitum. Our previous studies using the same 3/1 CSR protocol used only male rats, due to the requirement of stable background in sleep patterns (without reproductive hormone-dependent fluctuations) over at least 1 or 2 weeks [17–19, 24]. Due to similar requirements, we limited the present study to male rats. All animals were handled in accordance with the guidelines of the Canadian Council on Animal Care, and the animal handling protocols were approved by the Dalhousie University Committee on Laboratory Animals.

Six experiments were conducted. In Experiments 1–6 (see below), rats were randomly assigned to two to four experimental groups and run in multiple cohorts of six rats at a time (exceptions: four or six rats per cohort in Experiment 2; three or six rats per cohort in Experiment 6).

The 3/1 CSR protocol

The sleep restriction (SR) protocol involved housing rats individually in programmable, motorized activity wheels, as described previously [17]. Briefly, sleep was restricted by continuous cycles of 3 h of sleep deprivation, imposed by the slow rotation of the activity wheel (~2.5 m/min), followed by 1 h of sleep opportunity when the wheel remained stationary; the protocol (the first sleep deprivation period) began at the onset of the light phase, i.e. 07:00 am. Control rats were housed in the same wheel-chambers, but their activity wheels were always locked to allow undisturbed sleep (locked wheel or LW condition).

All rats underwent 4 or 5 days of habituation in LWs prior to their respective experimental protocols (Experiments 1–6). The rats in the CSR condition were additionally habituated to the rotation of the wheels at a speed of approximately 2.5 m/min for 5–20 min once a day during the light phase; the wheels were otherwise locked.

Rats had ad libitum access to food and water throughout the experiment. Their body weights were recorded on the last day of habituation and immediately after their respective protocols (Experiments 1–6).

Experiment 1: Iba1 immunohistochemistry

Treatment groups

Rats were assigned to four groups: two SR groups underwent the 3/1 CSR protocol for either 27 h (SR2, n = 9) or 99 h (SR5, n = 8), and two LW control groups (LW2, n = 8; LW5, n = 4) were housed, and left undisturbed, in locked activity wheels for time intervals matched to those of the SR2 and SR5 groups, respectively.

Perfusion and brain sectioning

At the end of their respective experimental protocols (i.e. 10:00 am), rats were given an overdose of an anesthetic mixture (208 mg/kg ketamine, 9.6 mg/kg xylazine, and 1.8 mg/kg acepromazine, IP). Animals were perfused intracardially with 100 mL of phosphate-buffered saline (pH 7.4), followed by 400 mL of 4% paraformaldehyde in 0.1 M phosphate buffer (pH 7.4).

Brains were post-fixed in the same fixative solution for 4–5 h, followed by cryoprotection in 30% sucrose in 0.01 M phosphate buffer at 4°C for 2–4 days. A freezing microtome was used to cut each brain into five series of 40 µm thick coronal sections, which were collected in 0.05 M Tris-buffered saline (TBS; pH 7.2–7.4).

Immunohistochemistry

Single-label immunohistochemistry for Iba1 was performed on one series of sections using a standard avidin–biotin–horseradish peroxidase complex (ABC) method as previously described [29], with a polyclonal rabbit anti-Iba1 antibody (1:2,000; Supplementary Table 1), a biotinylated donkey anti-rabbit IgG antibody (1:1,000; Jackson Laboratories), ABC (1:200, ABC Elite PK-6100; Vector Laboratories, Burlingame, CA), and diaminobenzidine in the presence of nickel ammonium sulfate and hydrogen peroxide.

Image acquisition

Image capture and analysis were conducted by an examiner (S.H.) who was blind to the treatment conditions. Two adjacent sections within the series (i.e. 200 µm apart) per rat were selected for quantitative analyses of Iba1 immunoreactivity in each of the following 10 brain regions known to be involved in sleep/wake, limbic, and autonomic functions [30]: the prelimbic cortex, anterior cingulate cortex, paraventricular hypothalamic nucleus, central amygdala, dentate gyrus of the hippocampus, perifornical lateral hypothalamic area, dorsal raphe nucleus, parabrachial nucleus, locus coeruleus, and the nucleus of the solitary tract (for respective anteroposterior levels, see Supplementary Table 2). Unilateral images (1,300 × 1,030 pixels) of each region were captured using a 10× (cell counts) or 20× (densitometry and morphology) objective lens on a bright-field microscope (Zeiss AxioPlan MOT II) equipped with an AxioCam camera, with identical exposure and illumination settings for all images.

Densitometry and cell counts

The density of Iba1 immunoreactivity and counts of Iba1-immunoreactive (ir) cells were obtained for each brain region unilaterally in two adjacent sections and averaged for each rat (see Supplementary Table 2 for analysis box sizes and locations).

ImageJ (NIH, Bethesda, MD; RRID: SCR_003070; www.imagej.net) was used to set two thresholds for Iba1 in each image, one for density of Iba1 immunoreactivity and the other for cell counts, as follows. For density, the pixel distribution from each image across a gray-scale spectrum ranging from 0 (black) to 255 (white) was first examined to determine the peak background gray value and the highest gray value (i.e. lightest) in the image. The difference between these two values was then subtracted from the peak background gray value to obtain a threshold to define positive Iba1 staining. All gray values below this threshold (i.e. darker) were considered immunopositive. A pilot analysis showed that this procedure adequately highlighted both processes and cell bodies that were visually judged to be stained for Iba1 and also normalized background staining intensity across sections and animals. The density of Iba1 immunoreactivity in each brain region was then calculated as the percentage of Iba1-ir area, by dividing the number of pixels that were below the threshold gray value by the total number of pixels within the analysis box. Pixels corresponding to blood vessels within the analysis box were excluded from the total pixel count.

For Iba1 cell counts, the threshold was set at 50% of the threshold for density described above, to highlight only Iba1-ir cell bodies, which were typically darkly stained. This setting eliminated processes as they were generally less darkly stained than cell bodies. The total number of Iba1-ir cells within respective analysis boxes was automatically counted in ImageJ, after excluding elements smaller than 20 µm^2.

Experiment 2: Microglia proliferation

Treatment groups

Rats were assigned to SR5 (n = 8) and LW5 (n = 8) groups.

CSR and bromodeoxyuridine injections

All rats received IP injections twice daily of 50 mg/kg bromodeoxyuridine (BrdU; Sigma-Aldrich, Oakville, ON) dissolved in saline [31], at 07:00 am and 03:00 pm (corresponding to the beginning of respective 3 h sleep deprivation periods), throughout the CSR or LW condition, with the final injection at 07:00 am on the last day of CSR/LW, for a total of nine injections. Immediately following the completion of their respective experimental protocols at 10:00 am, rats were anesthetized and perfused as described above under Experiment 1.

Tissue pretreatment and immunohistochemistry

Sections were incubated in 2N HCl for 30 min at 37°C to denature DNA, neutralized in sodium borate buffer (pH 8.5) for 10 min, and rinsed for 2 × 10 min in 0.05 M TBS, according to Junek et al. [32] with modification. Dual-label immunohistochemistry was conducted as previously described [32], using a polyclonal sheep anti-BrdU antibody (1:2,000; Supplementary Table 1), a polyclonal rabbit anti-Iba1 antibody (see Experiment 1 above), a Cy2-conjugated donkey anti-sheep IgG antibody (1:100; Jackson), and a Cy3-conjugated donkey anti-rabbit IgG antibody (1:400; Jackson). No BrdU immunolabeling was observed in an animal that did not receive BrdU injections. Visual inspection of brain sections confirmed that the tissue pretreatment did not appear to affect Iba1 immunostaining.

Image acquisition and analysis

For unilateral counts of double-labeled Iba1/BrdU-ir cells, two adjacent sections (200 µm apart) per rat were selected in each of the four brain regions that showed significant changes in Iba1 immunoreactivity following CSR (see Experiment 1: Iba1 immunohistochemistry in Results): the prelimbic cortex, central amygdala, perifornical lateral hypothalamic area, and dorsal raphe nucleus. Fluorescent images (2 µm z-stack; 1,024 × 1,024 pixels) were captured using a laser scanning confocal microscope (Zeiss LSM 510 Meta) and a 10× objective lens. The number of double-labeled Iba1/BrdU-ir cells was counted manually in each brain region using the same analysis boxes as described above under Experiment 1.

Experiment 3: Blood–brain barrier permeability

Treatment groups

Rats were assigned to SR5 (n = 6) and LW5 (n = 6) groups.

Evans Blue injection

Immediately following the SR5 or LW5 protocol (i.e. at 10:00 am), rats were anesthetized with an IP injection of ketamine (104 mg/

kg), xylazine (4.8 mg/kg), acepromazine (0.9 mg/kg) mixture, followed by an intracardiac injection of 2 mL/kg of 2% Evans Blue (EB) (Sigma-Aldrich) in saline. EB is a commonly used fluorescent tracer to assess blood–brain barrier permeability [33, 34]. The rats were then placed on a heating pad at 37°C to allow EB to circulate for 10 min under anesthesia [33]; the skin of the rats turned dark blue. Rats were then perfused as described above under Experiment 1. Brains were cut into 40 µm thick coronal sections using a freezing microtome and every fifth section was stored for the examination of perivascular leakage of EB.

Two additional rats served as controls. One LW5 rat was not injected with EB to serve as an EB-negative control. Another rat was perfused with a mixture of 4% paraformaldehyde and 1% EB following acute cryoinjury to the right frontoparietal cortex [35] to serve as a positive control for EB extravasation.

Histology

To visualize blood vessels, brain sections were incubated in fluorescein isothiocyanate (FITC)-conjugated tomato lectin (Sigma-Aldrich, Product #L0401, 20 µg/mL) in 1% bovine serum albumin in 0.05 M TBS for 2 h on a shaker at room temperature. Sections were then rinsed (3 × 10 min), mounted on gelatin-coated slides, and cover-slipped.

Image acquisition and analysis

Two adjacent sections (200 µm apart) per region per rat were selected for quantitative analyses in the prelimbic cortex and perifornical lateral hypothalamic area (see Supplementary Table 2 for analysis box sizes and locations). Unilateral images were captured using a 10× (prelimbic cortex) or 20× (perifornical lateral hypothalamic area) objective lens with an epifluorescence microscope (Zeiss Axiovert 200M) for EB (red) and FITC-conjugated tomato lectin (green).

Perivascular leakage of EB was assessed by subtracting the tomato lectin-positive blood vessels from the EB image, using Photoshop (Adobe; RRID: SCR_014199; www.adobe.com/products/photoshop.html). Specifically, each pixel gray value in the tomato lectin image was subtracted from the corresponding pixel gray value in the EB image to create a differential image. Next, using ImageJ, a histogram of the number of pixels at each gray-scale value between 0 (black) and 255 (white) was displayed for each differential image. The threshold value for positive EB fluorescence was defined as the highest gray value measured in the histogram for an EB-negative control image, corresponding to autofluorescence. Next, for each rat, the number of pixels with gray values greater (i.e. lighter) than the threshold was divided by the corrected total number of pixels (i.e. the total number of pixels minus the number of pixels occupied by blood vessels) in the image to obtain the percentage of EB-positive pixels (i.e. a measure of extravasation) for each differential image.

Experiment 4: Cytokine mRNA expression

Treatment groups

Rats were assigned to SR2 (n = 4), SR5 (n = 7), LW2 (n = 2), and LW5 (n = 5) groups.

At the end of their respective experimental protocols (i.e. 10:00 am), rats were deeply anesthetized with 5% isoflurane (in oxygen) and decapitated. Brains were immediately removed, and frontal cortex blocks were collected from both hemispheres by isolating the most anterior 5 mm portion of the frontal cortex, as described previously [19], and immediately frozen on dry ice and stored at –80°C.

RNA extraction and quantitative reverse transcriptase-polymerase chain reaction

Frontal cortex tissues were homogenized in TRIzol reagent (Ambion by Life Technologies, Carlsbad, CA). Total RNA was extracted using an Aurum Total RNA Fatty and Fibrous Tissue Pack (Bio-Rad, Catalog #732-6870, Hercules, CA) using the spin protocol according to the manufacturer's instructions. RNA quality and quantity were assessed using an Experion Bioanalyzer (Bio-Rad) and an Epoch microplate spectrophotometer (BioTek Instruments, Winooski, VT), respectively. Rats with poor RNA quality (Experion values below 6.5) were excluded from the experiment (n = 5 out of 18 rats). Total RNA samples were stored at –20°C prior to analysis.

Rat primers (Thermo Fisher Scientific, Waltham, MA) were used to detect the gene products for the inflammatory cytokines IL1β, TNFα, IL6, and IL10, as well as the three reference genes beta-2-microglobulin (β2M), glyceraldehyde-3-phosphate dehydrogenase (*GAPDH*), and hypoxanthine phosphoribosyltransferase (*HPRT*) (for primer sequences, see Supplementary Table 3). The expression stability of the three reference genes has previously been shown to be unaffected in rat brains by either 6 h of total sleep deprivation or 4 days of REM sleep deprivation [36]. Reverse transcriptase reactions were conducted using the iScript cDNA synthesis kit (Bio-Rad) using 1 µg of total RNA from each sample. qPCR was performed using SsoFast EvaGreen Supermix kit (Bio-Rad) with the CFX 96 Real-Time System C1000 Touch thermal cycler (Bio-Rad): 1 cycle of 30 s at 95°C followed by 40 cycles of 5 s at 95°C, 5 s at 55°C plus plate reading [37]. The melting curve consisted of 2 s stops at intervals of 0.5°C between 65°C and 95°C. All quantitative reverse transcriptase-polymerase chain reaction (qRT-PCR) analysis was performed according to MIQE guidelines [38]. Each sample was tested in triplicate and values were normalized to the three reference genes. Data analysis was performed with CFX Manager 3.1 software (Bio-Rad) using the ΔΔCq method.

Experiment 5: Microglia morphology

Treatment groups

Morphology analyses were conducted on Iba1-ir microglia in layers I and II/III of the prelimbic cortex, using sections that had been Iba1-immunostained for cell counts and densitometry in Experiment 1 (see above), for the SR2 (n = 9), SR5 (n = 8), LW2 (n = 5), and LW5 (n = 4) groups.

Cell selection and Sholl analysis

Layer I and layer II/III were delineated based on additional Iba1-immunostained sections that were counterstained for Nissl in a control rat. A grid of 50 × 50 µm^2 was placed over layer I and layer II/III, and 8–10 Iba1-ir cells in each layer were randomly selected unilaterally in two adjacent sections (200 µm apart) per rat. Only Iba1-ir cells with apparently intact processes that were not obscured by background labeling or other Iba1-ir cells were included in the analyses.

For Sholl analysis, the "concentric circles" plug-in in ImageJ was used to create a series of concentric circles centered at the

cell soma and radiating at 5 µm intervals [39]. The "cell counter" plug-in was used to mark each point where an Iba1-ir branch intersected a given circle. The following six parameters were calculated [40]: total number of intersections (between cellular processes and concentric circles), process maximum (maximum number of intersections at one radius), number of primary branches (number of branches that originate from the soma), ramification index (the process maximum divided by the number of primary branches), longest branch length, and cell soma size. The area of the cell soma was calculated using the threshold setting in ImageJ.

Experiment 6: Immunohistochemical characterization of microglia phenotype

Treatment groups

Rats were assigned to SR2 (n = 3), SR5 (n = 3), LW2 (n = 1), and LW5 (n = 2) groups.

Immunohistochemistry

To further characterize the molecular phenotype of microglia following CSR, sections through the frontal cortex were double labeled with a guinea pig anti-Iba1 antibody (1:1,000) and one of the following antibodies (see Supplementary Table 1): a polyclonal rabbit anti-P2Y12 receptor antibody (1:500) to label the purinergic P2Y12 receptor as a specific microglial marker expressed only under physiological conditions [27]; monoclonal mouse anti-CD68 (1:100) and anti-OX6/MHCII (1:500) antibodies for pro-inflammatory (often referred to as "M1") markers; and polyclonal rabbit anti-Arginase-1 (1:100), anti-cyclooxygenase-2 (1:200), or anti-mannose receptor/CD206 (1:100) antibodies for anti-inflammatory (often referred to as "M2") markers [26]. Cy2-conjugated donkey anti-guinea pig IgG (1:100; Jackson), Cy3-conjugated donkey anti-rabbit IgG (1:200; Jackson), and Cy3-conjugated donkey anti-mouse IgG (1:400; Jackson) were used as secondary antibodies. Double-label immunofluorescence using the guinea pig anti-Iba1 antibody (1:1,000; used in this experiment) with the rabbit anti-Iba1 antibody (1:2,000; used in Experiment 1, see above) showed a virtually complete overlap of microglia staining for both cell bodies and processes in the cortex (data not shown). A z-stack of 0.5 µm optical sections was collected through the prelimbic cortex for each animal using a 40× objective lens on a laser scanning confocal microscope (Zeiss LSM510).

Statistics

Statistical analyses were conducted using GraphPad Prism 6 (GraphPad Software, Inc., La Jolla, CA; RRID: SCR_002798; www.graphpad.com). In Experiments 1, 4, and 6, one- or two-way analyses of variance (ANOVA) were performed to compare treatment groups, followed, when applicable, by Fisher's LSD post hoc tests. When the data did not meet the assumptions of the ANOVA, Kruskal–Wallis tests were used, followed, when applicable, by Dunn's multiple comparison tests. In Experiments 2 and 3, two-tailed, unpaired Student's t-tests or, when the data showed heterogeneity of variance, Mann–Whitney U-tests were used. Probability values of <0.05 were considered statistically significant. Data values are expressed as means ± standard error of the mean (SEM).

Results

Experiment 1: Iba1 immunohistochemistry

The SR2 (n = 9) and SR5 (n = 8) groups underwent 27 and 99 h, respectively, of the 3/1 CSR protocol. The non-sleep-deprived control groups LW2 (n = 8) and LW5 (n = 4) were kept in LWs for corresponding intervals. The LW2 and LW5 groups did not significantly differ between each other in either the number of Iba1-ir cells or the density of Iba1 immunoreactivity in any of the brain regions examined (p = 0.20–0.84); therefore, they were combined into a single control group (LW).

Iba1 immunoreactivity

Iba1 immunoreactivity was analyzed in 10 brain regions with sleep/wake, limbic, and autonomic functions. In 4/10 regions examined, including the prelimbic cortex, central amygdala, perifornical lateral hypothalamic area, and dorsal raphe nucleus, the number of Iba1-ir cells and/or the density of Iba1 immunoreactivity changed in response to CSR. Figure 1 shows examples of Iba1 immunoreactivity in these four "CSR-responsive" regions. Most microglia in all treatment groups appeared ramified rather than ameboid, with relatively small cell bodies and many fairly long and branching processes (Figure 1).

In the prelimbic cortex, Iba1 immunoreactivity was increased after both 27 (SR2) and 99 h (SR5) of CSR. Specifically, the number of Iba1-ir cells (Figure 2, A) was higher in the SR2 than LW group (+137%, p = 0.017) and remained elevated in the SR5 group (+99% vs LW, p = 0.045; main effect of group: $F_{2,25}$ = 3.55, p = 0.044). Similarly, the density of Iba1 immunoreactivity (Figure 2, B) was increased in the SR2 (+57% vs LW, p = 0.011) and SR5 groups (+61% vs LW, p = 0.009; $F_{2,25}$ = 5.43, p = 0.011).

In the other three CSR-responsive brain regions, Iba1 immunoreactivity was increased only after 99 h of CSR (SR5). In the central amygdala, Iba1-ir cell counts (Figure 2, D) tended to increase in the SR5 group (+197% vs LW; +191% vs SR2), although there was no significant group difference (H = 3.74, p = 0.15). The density of Iba1 immunoreactivity (Figure 2, E) was significantly increased in the SR5 group (+71% vs LW, p = 0.028; +85% vs SR2, p = 0.017; $F_{2,25}$ = 4.15, p = 0.028).

In the perifornical lateral hypothalamic area, the number of Iba1-ir cells (Figure 2, G) was significantly increased in the SR5 group (+227% vs LW, p = 0.015; +175% vs SR2, p = 0.039; $F_{2,26}$ = 3.76, p = 0.037). The density of Iba1 immunoreactivity (Figure 2, H) was not significantly changed by CSR ($F_{2,26}$ = 1.62, p = 0.22), although it tended to be increased in the SR5 group (+49% vs LW).

In the dorsal raphe nucleus, Iba1-ir cell counts tended to be increased in the SR5 group (+103% vs LW; +179% vs SR2; $F_{2,26}$ = 3.23, p = 0.056; Figure 2, J). The density of Iba1 immunoreactivity (Figure 2, K) was significantly higher in the SR5 than LW group (+67%, p = 0.0072; $F_{2,26}$ = 4.27, p = 0.025).

Positive correlations were found between the number of Iba1-ir cells and the density of Iba1 immunoreactivity in all of the four CSR-responsive brain regions (Figure 2, C, F, I, and L; r = 0.68–0.88, all p < 0.0001, n = 28 or 29/region).

In the other six brain regions examined, there was no significant effect of CSR (Supplementary Table 4). Nonetheless, the highest number of Iba1-ir cells and/or density of Iba1 immunoreactivity was observed in the SR2 or SR5 group in all these regions, with a trend for an increase in Iba1 density in the SR2 group in the locus coeruleus (p = 0.0503 for the main effect of treatment).

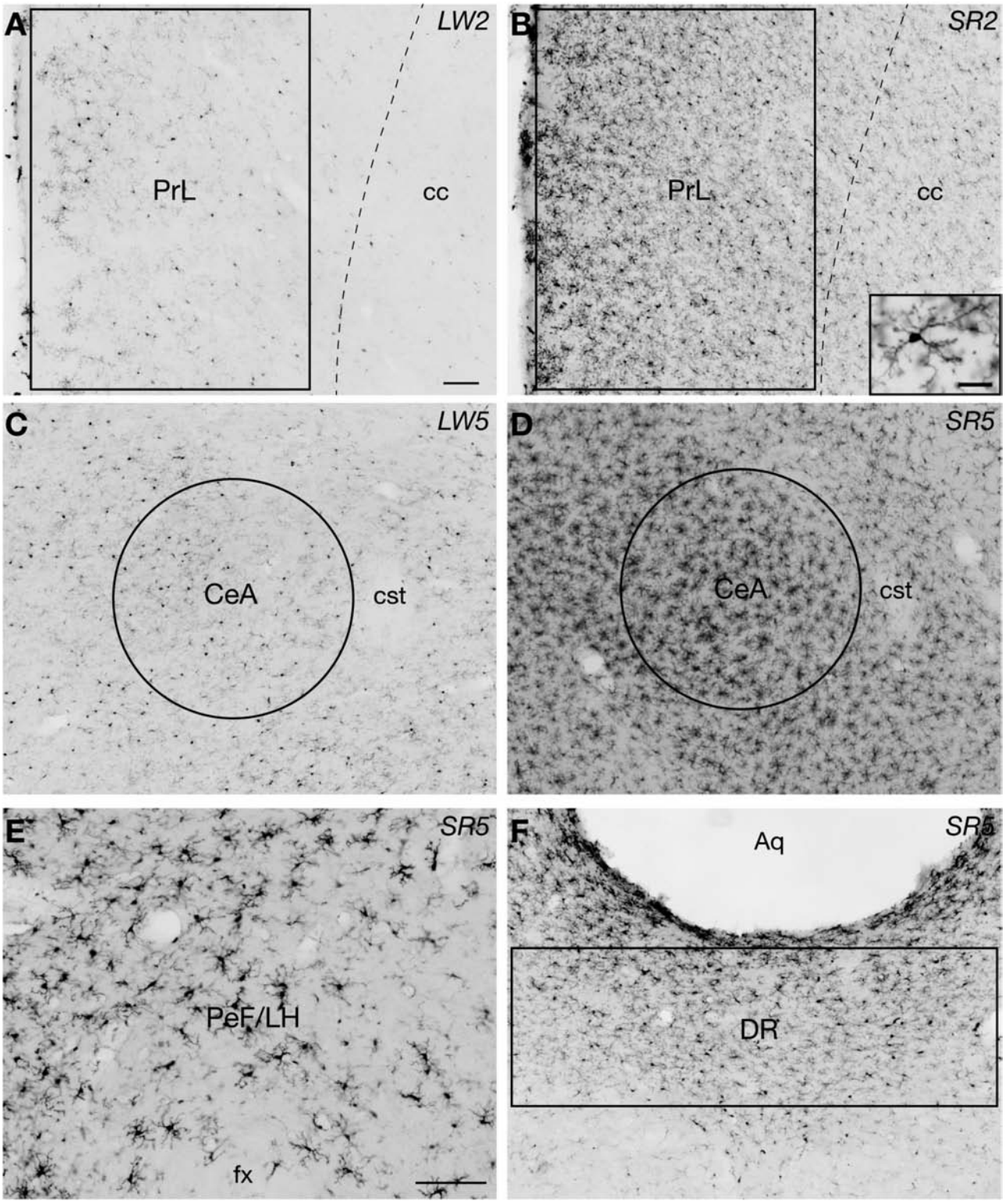

Figure 1. Examples of Iba-1 immunoreactive (-ir) microglial cells in the four brain regions that showed significant increases in Iba1 immunoreactivity during and following chronic sleep restriction (CSR), including the prelimbic cortex (PrL; A and B including an inset), central amygdala (CeA; C and D), perifornical lateral hypothalamic area (PeF/LH; E), and dorsal raphe nucleus (DR; F). The sections shown in A and C are from rats in the locked wheel control groups LW2 and LW5, respectively. The section shown in B is from a rat in the SR2 group that underwent 27 h of the 3/1 CSR protocol, and the sections shown in D–F are from rats in the SR5 group that underwent 99 h of the same protocol. The size and placement of analysis boxes or circles used for quantification of Iba1 immunoreactivity are shown for each region (in E, the entire image was used for analyses). Aq, cerebral aqueduct; cc, corpus callosum; cst, commissural stria terminalis; fx, fornix. Scale bars = 100 μm (A–F) and 20 μm (inset in B).

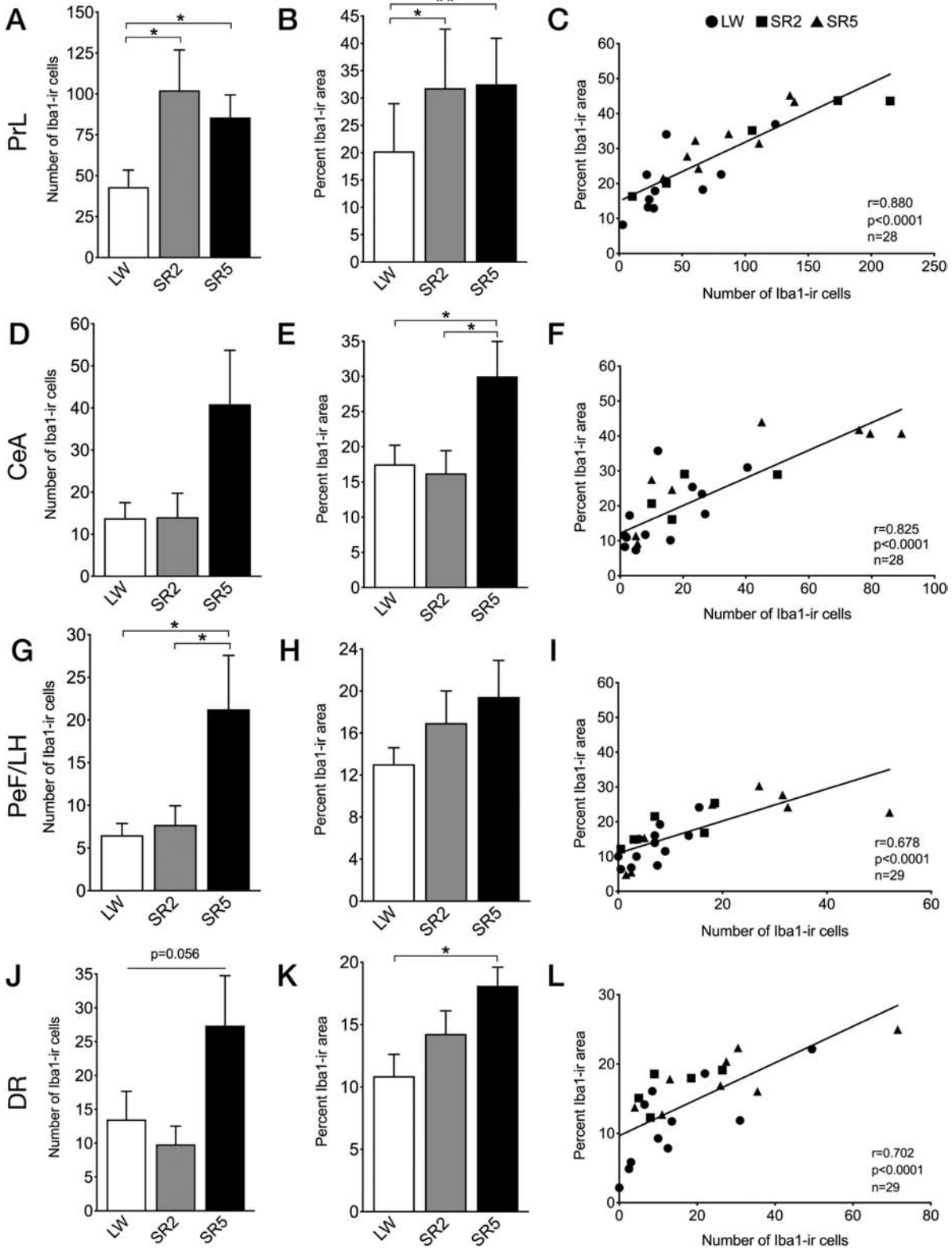

Figure 2. The number of Iba1-ir cells (*left*), density of Iba1 immunoreactivity (*middle*), and scatterplots of the density versus cell counts (*right*), in the four brain regions that showed significant increases in Iba1 immunoreactivity during and/or following CSR, including the prelimbic cortex (PrL; A–C), central amygdala (CeA; D–F), perifornical lateral hypothalamic area (PeF/LH; G–I), and dorsal raphe nucleus (DR; J–L). Data are shown as means ± SEM for the LW (n = 4), SR2 (n = 8 or 9), and SR5 (n = 8) groups. The LW2 and LW5 control groups were combined into a single LW group (n = 11 or 12). Cell counts are obtained from respective analysis boxes and are expressed per section per side of the brain. Regression lines are shown as solid lines. $^{*}p < 0.05$, $^{**}p < 0.01$ (Fischer's LSD post hoc tests).

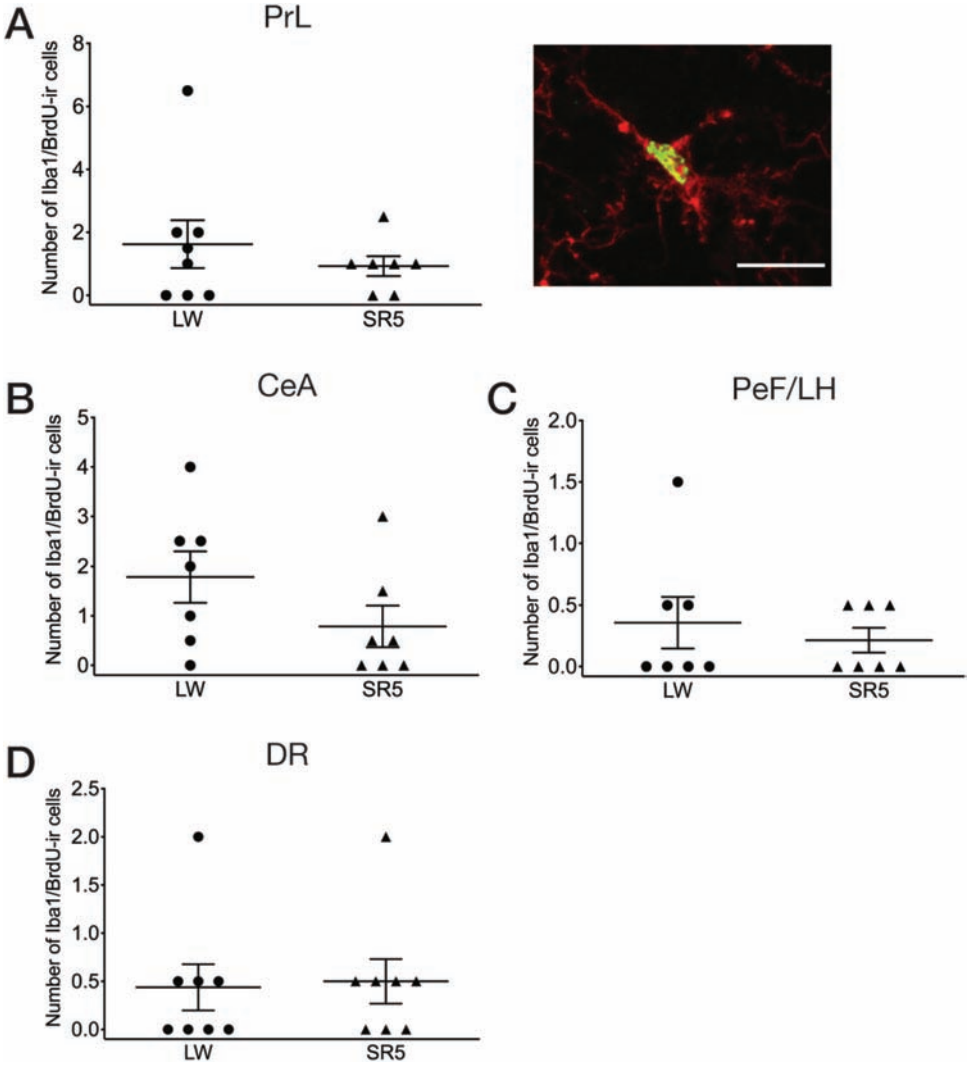

Figure 3. Number of double-labeled Iba1 (red)/BrdU (green) -ir cells in the prelimbic cortex (PrL; A), central amygdala (CeA; B), perifornical lateral hypothalamic area (PeF/LH; C), and dorsal raphe nucleus (DR; D), that is, the four brain regions that showed an increase in Iba1 immunoreactivity in response to CSR (see Figure 2). An example of double-labeled microglia (green nucleus for BrdU, and red cytoplasm for Iba1) in the PrL is shown in A, right. Scale bar = 20 µm. Mean values (±SEM) are shown for the LW5 (n = 7 or 8) and SR5 (n = 7 or 8) groups. Each symbol represents a rat. CSR did not significantly affect the number of double-labeled Iba1/BrdU-ir cells in any of these regions (unpaired t-tests).

Body weight

The average percent change in body weight from pre-protocol levels varied among the LW2, LW5, SR2, and SR5 groups ($F_{3,22}$ = 14.35, p < 0.0001; Supplementary Table 5). Specifically, the LW2 and LW5 groups progressively gained body weight (+3.3% and +9.5%, respectively), while the SR2 and SR5 groups increasingly lost weight (–3.3% and –7.7%, respectively).

Experiment 2: Microglia proliferation

To evaluate the possibility that the proliferation of resident microglia contributed to the observed increase in the number of Iba1-ir cells following CSR (see Experiment 1 above), we assessed for the incorporation of the cell division marker BrdU in Iba1-ir cells using double immunofluorescence, in the prelimbic cortex, central amygdala, perifornical lateral hypothalamic area, and dorsal raphe nucleus in an additional cohort of SR5 (n = 7 or 8) and LW5 (n = 8) animals that received BrdU injections (see Experiment 2 in Methods for injection paradigm). There were only a few Iba1/BrdU-ir cells in each of these four brain regions in both groups, with no significant group difference (p = 0.16–0.85; Figure 3). As a positive control, BrdU-ir cells were present in the dentate gyrus of the hippocampus and subventricular zone of the lateral ventricle in both groups (data not shown) [32].

Similar to Experiment 1, the SR5 group lost weight from pre-protocol levels (–5.4%) while the LW5 group gained weight (+10.5%; SR5 vs LW5, p < 0.0001; Supplementary Table 6).

Experiment 3: Blood–brain barrier permeability

Next, to determine whether or not peripheral macrophage recruitment through the blood–brain barrier contributed to the increases in the number of Iba1-ir cells observed following CSR (see Experiment 1 above), we examined blood–brain barrier permeability by assessing the leakage of the fluorescent dye EB into the brain parenchyma following intracardiac

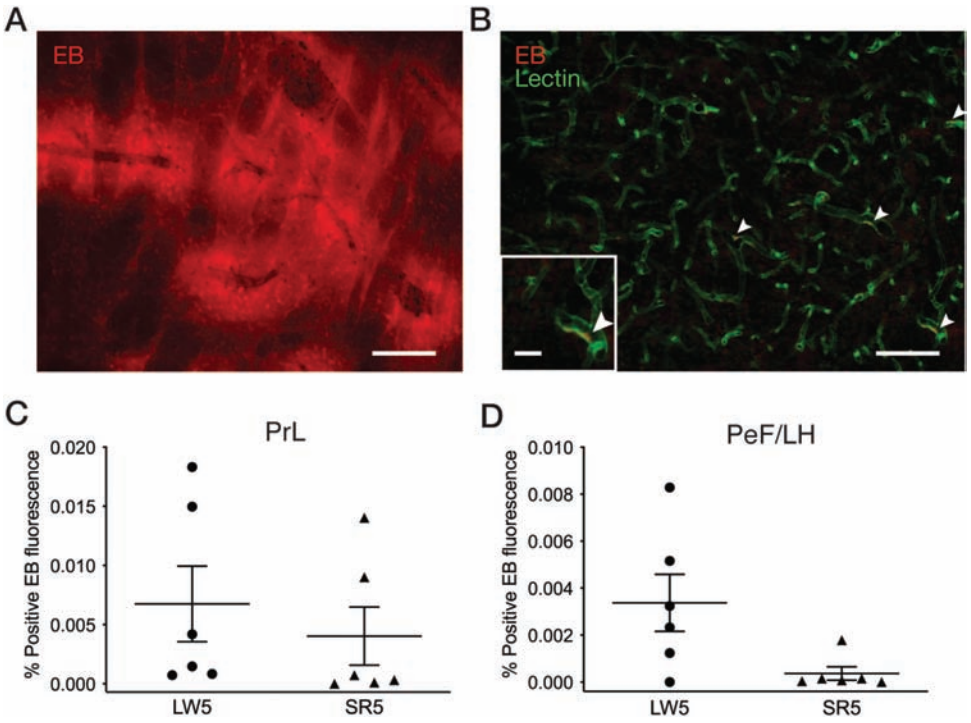

Figure 4. Quantification of Evans Blue (EB) dye fluorescence in brain tissue following CSR. (A) Example of a fluorescent microscope image showing EB extravasation (red) in the striatum of a positive control rat with cryoinjury. Scale bar = 150 µm. (B) Example of a fluorescent microscope image in the prelimbic cortex (PrL) of an SR5 rat showing blood vessels identified with tomato lectin-FITC (green) and EB (red). White arrowheads indicate EB remaining inside blood vessels; no EB fluorescence was observed outside of blood vessels. Scale bars = 100 µm and 25 µm (inset). EB fluorescence was quantified in the PrL (C) and perifornical lateral hypothalamic area (PeF/LH; D) for the SR5 ($n = 6$) and LW5 ($n = 6$) groups. Each symbol represents a rat. See Experiment 3 in Methods for calculation of percent positive EB fluorescence area. CSR did not have a significant effect on the percent positive EB fluorescence area in either the PrL or PeF/LH (unpaired *t*-tests).

injection in an additional cohort of SR5 ($n = 6$) and LW5 ($n = 6$) animals. Two additional animals served as EB-positive and negative controls (see Experiment 3 in Methods for specific treatment procedures).

As shown in Figure 4, A, in the EB-positive control rat, clear extravasation of EB was observed in various brain regions (e.g. cortex, striatum, and hippocampus), while in the EB-negative control rat, no EB fluorescence was visible as expected (not shown). In the LW5 and SR5 groups, no EB fluorescence was seen outside of blood vessels defined by tomato lectin binding in any brain region examined, although some residual EB inside blood vessels was occasionally observed (Figure 4, B; white arrowheads).

Consistent with these observations, the quantification of EB extravasation indicated that the percentage of pixels with positive EB fluorescence was 12.6% in the striatum of the EB-positive control but very low (<0.02%) in the LW5 and SR5 groups, with no significant group difference, in the prelimbic cortex ($t_{10} = 0.67$, $p = 0.51$; Figure 4, C) and perifornical lateral hypothalamic area ($U = 6.5$, $p = 0.074$; Figure 4, D).

As in Experiments 1 and 2, the SR5 group lost body weight from pre-protocol levels (–10.5%) while the LW5 group gained weight (+5.1%; SR5 vs LW5, $p = 0.0003$; Supplementary Table 7).

Experiment 4: Cytokine mRNA expression

Next, to determine whether the increase in Iba1 immunoreactivity following CSR is accompanied by changes in the expression of inflammatory cytokines, we examined the mRNA levels of TNFα, IL1β, IL6, and IL10 in the frontal cortex (including the prelimbic cortex) following CSR. The frontal cortex was selected because it is known to be sensitive to sleep loss [41] and has been shown to respond to the 3/1 CSR protocol with increased BDNF protein levels [19] and to a different CSR protocol with increased IL1β and TNFα mRNA levels [42]. After the exclusion of five rats due to poor RNA quality (see Experiment 4 in Methods), the final animal numbers in each group for qRT-PCR analysis were SR2 ($n = 4$), SR5 ($n = 5$), LW2 ($n = 2$), and LW5 ($n = 2$). There was no obvious group difference between the LW2 and LW5 groups for any cytokine mRNA levels, and thus these two control groups were combined into a single LW group.

The LW, SR2, and SR5 groups did not significantly differ in the normalized mRNA levels of TNFα ($H = 1.53$, $p = 0.49$; Figure 5, A), IL1β ($H = 0.74$, $p = 0.72$; Figure 5, B), and IL6 ($H = 0.17$, $p = 0.92$; Figure 5, C). In contrast, normalized IL10 mRNA levels were significantly different between the three treatment groups ($H = 7.14$, $p = 0.017$; Figure 5, D): IL10 mRNA levels were higher in the SR2 group than the LW group ($p = 0.041$) and were at the control levels in the SR5 group ($p > 0.99$ vs LW).

As in Experiment 1, the LW2 and LW5 groups gained body weight from pre-protocol levels (+5.5% and +12.5%, respectively; Supplementary Table 8), while the SR2 group lost weight (–4.3%). The SR5 group, however, did not lose weight as in the previous experiments but maintained pre-protocol levels (+0.7%). Nonetheless, this was in contrast to the significant body weight gain observed in the LW5 group ($p = 0.0062$ vs SR5; Supplementary Table 8).

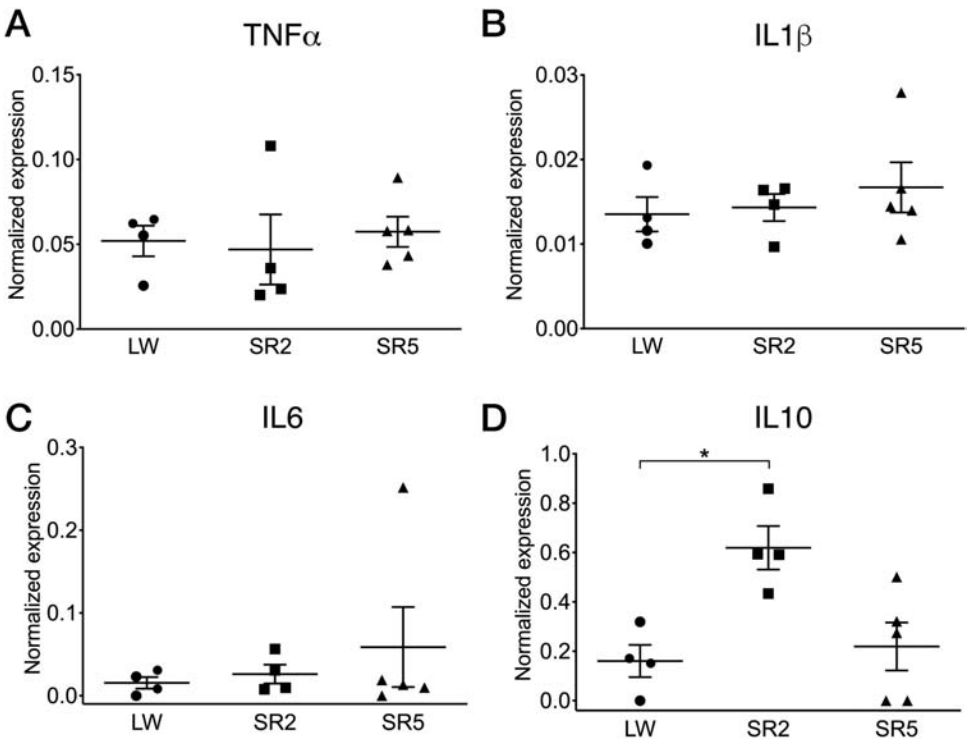

Figure 5. Cytokine expression in the frontal cortex under CSR and control conditions. Normalized mRNA levels (mean ± SEM) of tumor necrosis factor-α (TNFα; A), interleukin-1β (IL1β; B), IL6 (C), and IL10 (D) are shown for the LW (n = 4), SR2 (n = 4), and SR5 (n = 5) groups. Each symbol represents a rat. The LW2 and LW5 control groups were combined into a single LW control group. While TNFα, IL1β, and IL6 mRNA levels were not affected by CSR, IL10 mRNA levels were significantly increased in the SR2 group compared to the LW group and were at control levels in the SR5 group. *$p < 0.05$ (Dunn's multiple comparison test).

Experiment 5: Microglia morphology

Since the morphology of microglia changes according to their functional state [43], we quantitatively examined whether CSR induces changes in microglia morphology in the prelimbic cortex, the only region that showed an increase in Iba1 immunoreactivity after both 27 and 99 h of CSR (see Experiment 1 above). Previous studies reported changes in the density and morphology of Iba1-ir microglia in the prelimbic cortex following chronic stress exposure [44, 45]. Sholl analyses were conducted on randomly selected Iba1-ir cells in layer I and layer II/III in the SR2 (n = 9), SR5 (n = 8), LW2 (n = 5), and LW5 (n = 4) groups used in Experiment 1. As there was no significant difference between the LW2 and LW5 groups in any of the six morphological parameters analyzed (p = 0.14 to >0.99), these two control groups were combined into a single control group (LW).

The LW, SR2, and SR5 groups did not significantly differ in any morphological parameters in either of the two cortical layers ($F_{2,44}$ = 0.24–1.63, p = 0.21–0.79), including soma size (Figure 6, A), total number of intersections (Figure 6, B), ramification index (Figure 6, C), process maximum (Supplementary Figure 1, A), number of primary branches (Supplementary Figure 1, B), and longest branch length (Supplementary Figure 1, C). When calculated as a function of distance from the cell soma, the number of intersections of microglia in layer I and layer II/III was also similar across groups (Supplementary Figure 1, D and E).

Irrespective of treatment groups, however, microglia were more ramified in layer I than in layer II/III of the prelimbic cortex. There was a main effect of layer for the total number of intersections (Figure 6, B), process maximum (Supplementary Figure 1, A), number of primary branches (Supplementary Figure 1, B), and longest branch length (Supplementary Figure 1, C; $F_{1,44}$ = 16.75–30.55, p <0.0001–0.0002). The main effect of layer did not reach statistical significance for soma size ($F_{1,44}$ = 3.25, p = 0.078; Figure 6, A) and ramification index ($F_{1,44}$ = 2.97, p = 0.092; Figure 6, C).

As another way to assess for differences in the degree of ramification between the treatment groups, all microglia from all the treatment groups were pooled together, ranked based on their ramification index value, and divided into quartiles (from less ramified to more ramified), separately for layer I (Figure 6, D) and layer II/III (Figure 6, E) of the prelimbic cortex. Next, in each layer, the proportion (percentage) of microglia within each quartile was calculated to obtain a population profile for each rat. These profiles were then statistically compared between the three treatment groups. A repeated-measures two-way ANOVA showed no main effect of group or quartile for either layer (p = 0.63–0.85), indicating that there was no significant group difference in the population profile for ramification in response to CSR in either layer of the prelimbic cortex.

Experiment 6: Immunohistochemical characterization of microglia molecular phenotype

Finally, we examined the molecular phenotype of microglia in the prelimbic cortex, where microglia morphology was quantified (see Experiment 5 above), in additional SR2 (n = 3), SR5 (n = 3), LW2 (n = 1), and LW5 (n = 2) animals. As shown in Figure 7, virtually all Iba1-ir microglia were strongly co-immunolabeled with P2Y12 receptors, and vice versa, in the prelimbic cortex of all treatment groups. However, within each microglial cell, Iba1 and P2Y12 staining did not completely overlap, consistent with the cytoplasmic and cell membrane localization, respectively, of Iba1 and P2Y12 receptors

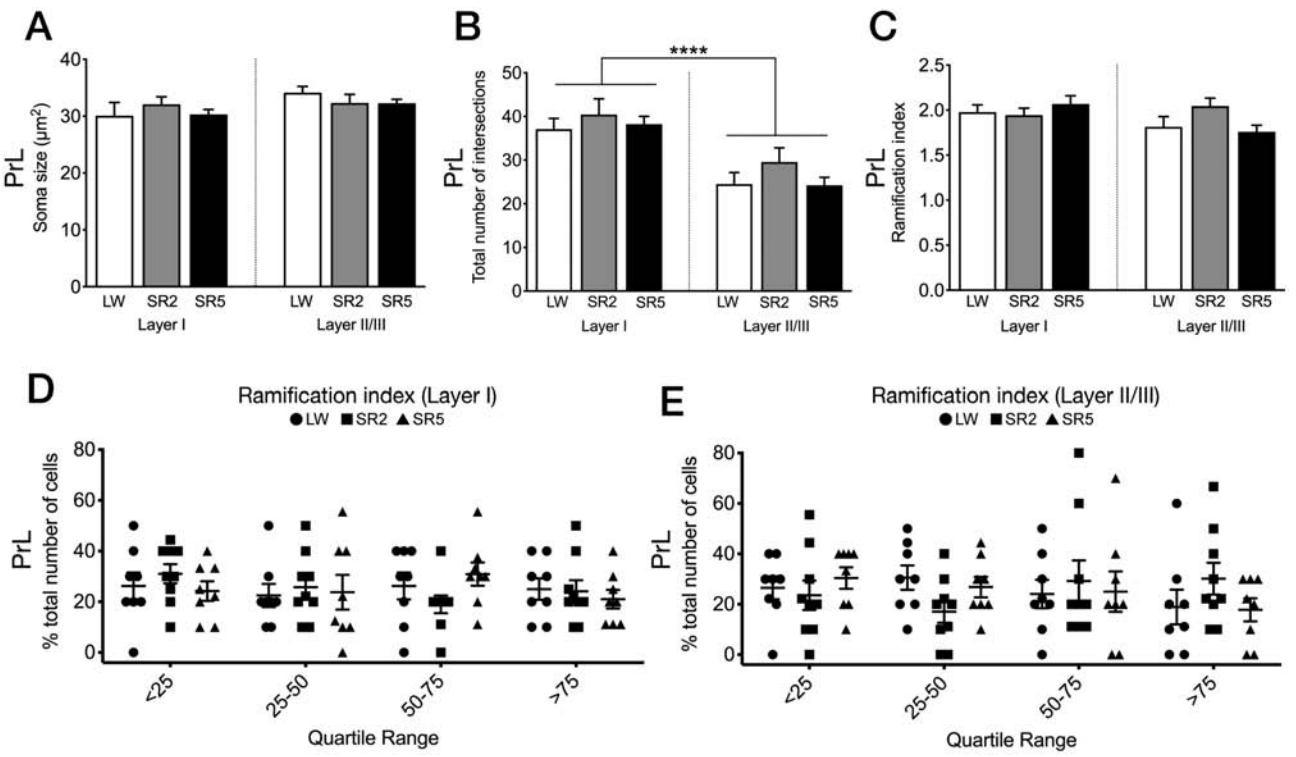

Figure 6. Morphological parameters of microglial cells in layers I and II/III of the prelimbic cortex (PrL), which showed a significant increase in Iba1 immunoreactivity after both 27 and 99 h of CSR (see Figure 2, A–C). Mean (+SEM) soma size (A), total number of intersections (B), and ramification index (C) are shown for the LW (n = 9), SR2 (n = 9), and SR5 (n = 8) groups. Microglia (n = 8–10/layer/rat) were randomly selected for Sholl analyses in each animal (see Experiment 1 in Methods for further details). The LW2 and LW5 control groups were combined into a single LW control group. (A–C) There was no significant effect of CSR on soma size (A), total number of intersections (B), or ramification index (C). However, the total number of intersections (B) was significantly greater in layer I (*left*) than in layer II/III (*right*) across all treatment groups. (D and E) All microglia across animals were pooled, ranked, and divided into quartiles from low to high ramification index, and the proportion of cells in each quartile was calculated for each animal in each treatment group for layer I (D) and layer II/III (E). No significant group difference was found in the proportions of microglia in each quartile in either layer. See Supplementary Figure 1 for additional morphological parameters analyzed. $^{****}p < 0.0001$ (main effect of layer, two-way repeated ANOVA).

[27, 46]. Thus, P2Y12 did not stain microglial cell bodies as distinctly as Iba1 did, while it revealed more complex secondary and tertiary branches than did Iba1. Exclusive presence of P2Y12 receptor immunoreactivity in Iba1-ir microglia and absence of P2Y12 labeling in Iba1-ir meningeal macrophages (Figure 7) are consistent with previous reports [27, 28].

Iba1-ir microglia in the prelimbic cortex were not immunoreactive for any of the pro- (CD68 and OX6) or anti- (arginase-1, cyclooxygenase-2, and mannose receptor) inflammatory markers examined in all treatment groups (Supplementary Figure 2). Iba1-ir meningeal macrophages, however, were co-labeled with all these inflammatory markers (Supplementary Figure 2), as has been previously reported [47–49], except arginase-1. Additionally, as reported previously [50–54], immunolabeling of arginase-1, cyclooxygenase-2, and mannose receptor, but not CD68 and OX6, was found in frontal cortex neurons (Supplementary Figure 2).

Compared to pre-protocol levels, the LW2 and LW5 groups gained body weight (+3.7% and +7.3%, respectively), the SR2 group did not gain weight (+0.1%), and the SR5 group lost weight (–10.4%; Supplementary Table 9).

Discussion

We show here that 27 and 99 h of the 3/1 CSR protocol increased the number of Iba1-ir microglia and the density of Iba1 immunoreactivity in selected sleep/wake and limbic brain regions in adult rats. Despite the observed increases in Iba1 immunoreactivity, microglia morphology examined in the prelimbic cortex was unaffected by CSR, with no change in cell body size or degree of ramification. Consistent with the lack of morphological changes, cortical microglia were also immunoreactive for P2Y12 receptors but not for several pro- or anti-inflammatory markers examined, suggesting a physiological or homeostatic microglial phenotype. Furthermore, cortical mRNA levels of several pro-inflammatory cytokines were not affected by CSR, while mRNA levels of the anti-inflammatory cytokine IL10 were transiently increased after 27 h of CSR.

CSR caused a gradual loss of body weight compared to pre-protocol levels. This modest weight loss is consistent with previous reports using the same [17, 19, 24] or different [55, 56] CSR protocols in rats. As reported previously in another CSR study [56], the weight loss in SR rats may reflect a negative energy balance associated with hyperphagia, although food intake was not measured in the present study.

Methodological considerations and limitations

A control group experiencing the same number of wheel rotations as those in the sleep-restricted groups but with minimal or no sleep deprivation was not included in the present study. Therefore, we cannot rule out that the increased locomotor activity inherent to the CSR protocol contributed, at least in part, to the observed changes in Iba1 immunoreactivity in response

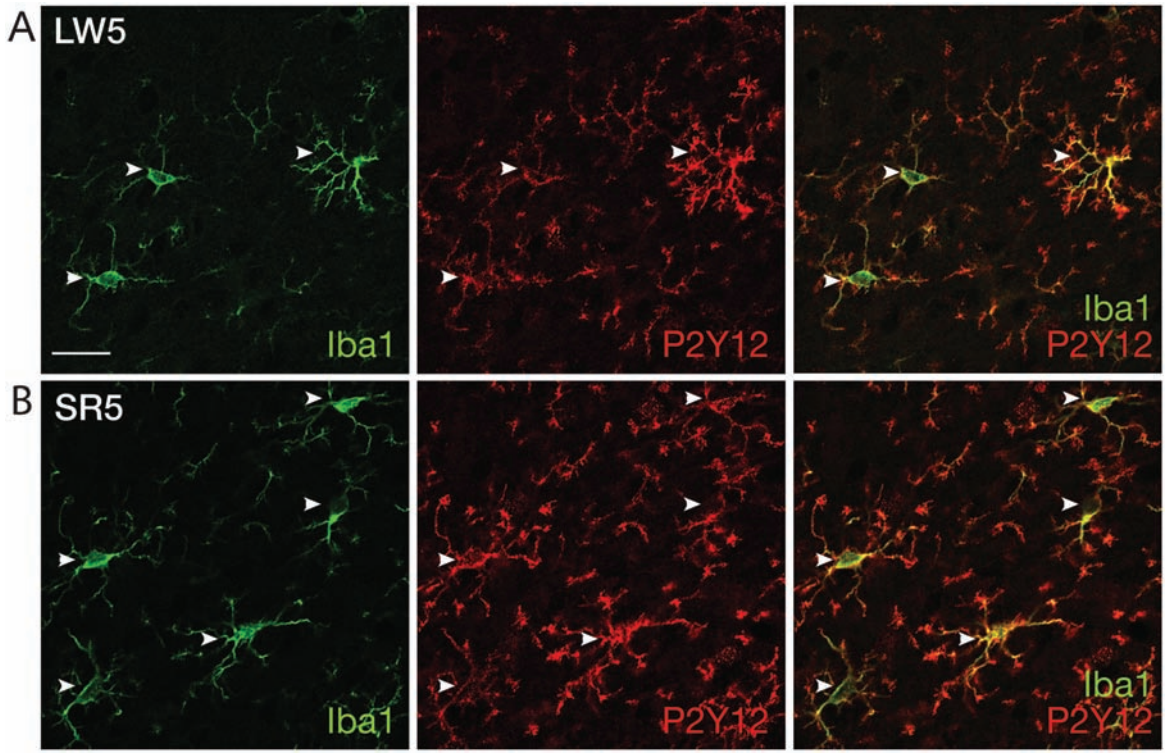

Figure 7. Representative confocal images of double-labeled immunofluorescence for Iba1 (green) and P2Y12 receptors (red) in the prelimbic cortex of LW5 (A) and SR5 (B) rats. White arrowheads indicate individual microglia co-labeled with Iba1 and P2Y12 receptors in both rats. Scale bar = 20 μm.

to CSR. However, we suspect that this is unlikely for the following reasons: First, 27 h of CSR did not significantly increase Iba1 immunoreactivity above control levels in any of the regions examined except the prelimbic cortex, suggesting no general acute effect of locomotor activity on Iba1 immunoreactivity. Second, forced locomotion for 20 min daily over 2 weeks reduced ischemia-induced increases in Iba1 immunoreactivity in the rat hippocampus [57], and voluntary wheel running for 10 days did not alter the number or the morphology of Iba1-ir cells in the mouse hippocampus [58]. In addition, there is little evidence to support that increased locomotion associated with wheel rotations contributed to the lack of changes in pro-inflammatory cytokine expression in the frontal cortex following CSR. Specifically, a previous study [59] reported that 7 weeks of forced treadmill running for 1–2 h/day reduced sleep deprivation-induced IL1β mRNA levels in the hippocampus but not in the frontal cortex in rats; neither treadmill running nor sleep deprivation affected TNFα and IL6 mRNA levels in either region [59].

Another issue to consider is the possibility that stress inherent to the 3/1 CSR protocol contributed to the observed increases in Iba1 immunoreactivity. Previous studies using a 20/4 CSR protocol in rats reported that plasma corticosterone levels were mildly increased at the end of daily 20 h sleep deprivation (using slowly rotating wheels) followed by a return to control levels at the end of the subsequent 4 h sleep opportunity [55, 60, 61]. However, we are inclined to believe that, between the two types of protocol, the 3 h sleep deprivation/1 h sleep opportunity cycle is less stressful and, therefore, would have less of an effect on corticosterone levels, although corticosterone levels were not measured in the present study. Highly stressful experiences such as repeated psychosocial stress for 6 days in mice [62] or 14 days in rats [45] did produce distinct morphological changes in microglia with hypertrophy combined with shorter, thickened processes consistent with pro-inflammatory activation [62]. Thus, we suppose that the stress associated with the 3/1 CSR protocol was likely mild, although we cannot exclude its possible contribution to the increased Iba1 immunoreactivity following CSR. More plausibly, however, the increases in Iba1 immunoreactivity and the lack of morphological change in microglia suggest a homeostatic or "adaptive" response to CSR.

Finally, although the changes in Iba1 immunoreactivity observed in response to CSR in the present study were clear and fairly robust, the use of additional immunohistochemical markers that recognize microglia in all functional phenotypes, such as TMEM119 [63] and CD11b [64], would have strengthened our results. In addition, further validation of the changes in Iba1 immunoreactivity using Western blot would be useful.

Region-specific increases in Iba1 immunoreactivity in response to CSR: lack of proliferation, recruitment, or morphological changes

The 3/1 CSR protocol increased Iba1 immunoreactivity with different time courses in 4 out of the 10 examined brain regions with sleep/wake regulatory and limbic functions. In the prelimbic cortex, the number of Iba1-ir cells and/or the density of Iba1 immunoreactivity increased after 27 h of CSR and remained elevated after 99 h of CSR, while in the central amygdala, perifornical lateral hypothalamic area, and dorsal raphe nucleus, increases were observed only after 99 h of CSR. The increase in Iba1 immunoreactivity, however, was not universal; in fact, 6 out of the 10 brain regions examined in the present study showed no significant changes. These included the lateral parabrachial

nucleus and locus coeruleus, which are involved in sleep/wake regulation [30], as well as the anterior cingulate cortex, paraventricular hypothalamic nucleus, nucleus of the solitary tract, and dentate gyrus of the hippocampus. We did not examine microglia morphology in these regions and cannot rule out the possibility that these microglia responded to CSR with morphological changes without changing their Iba1 immunoreactivity. Nonetheless, the lack of change in Iba1 immunoreactivity in the hippocampus in response to CSR is consistent with the previously reported lack of change in the density of Iba1-ir cells in the mouse hippocampus after 72 h of REM sleep deprivation [12]. However, this result contrasts with previously reported increases in the number of cells immunopositive for Iba1 or another microglial marker OX-42 in the hippocampus after 5 days of sleep fragmentation in rats [11] and after either 1 day or 1 week after 24 h of sleep disruption in mice [15]. Collectively, we believe that the regionally different levels or time courses of microglia response likely reflect different functions of these brain areas and different roles microglia play in them.

Although microglia are known to proliferate rapidly in response to a variety of stimuli [65], proliferation (examined using BrdU) did not appear to contribute to the observed increase in the number of Iba1-ir microglia in any of the four CSR-responsive brain regions. Similarly, a previous study reported no evidence of microglia proliferation in response to approximately 2 weeks of chronic stress in stress-related brain regions in rats [66]. Additionally, we found no evidence for blood–brain barrier disruption (using EB) in response to CSR, suggesting that macrophage recruitment is an unlikely explanation for the increased number of Iba1-ir cells, despite reports of increased blood–brain barrier permeability to EB and other fluorescent tracers following sleep disruption for 6 days in mice [67] and 10 days in rats [33, 68]. The absence of infiltrating macrophages is further supported by our result that virtually all microglia contained P2Y12 receptors, a selective marker for homeostatic microglia [27, 28] (but see Ref. [69]), which is not expressed by macrophages recruited from the periphery [70]. Thus, the observed increases in Iba1-ir cell numbers in response to CSR are most likely due to an upregulation of Iba1 levels in existing microglia, rather than an actual increase in the number of microglial cells. Given the high mobility of microglia [71, 72], however, we cannot exclude the possibility that the migration of microglia from adjacent brain regions contributed to the increased numbers of Iba1-ir microglia in the CSR-responsive brain regions.

Despite the increases in Iba1 immunoreactivity in response to CSR, microglia in all CSR-responsive regions retained a ramified phenotype and a relatively small cell body size, indicative of a homeostatic or physiological state. When quantitatively analyzed in the prelimbic cortex, microglia morphometric measures showed no differences between the treatment groups. Additionally, the values of the morphological parameters analyzed in the current study for the prelimbic cortex are comparable to those reported in rats under control (no CSR) conditions [39, 40]. These results are in contrast to the previously reported increased proportion of less ramified microglia in response to 4.5 days of CSR in the frontal cortex of adolescent mice [10]. Differences in species, age, and/or protocols may account for this discrepancy.

Cytokine expression during CSR

In the frontal cortex, in parallel with the initial increase in Iba1 immunoreactivity, the mRNA level of the anti-inflammatory cytokine IL10 was transiently increased after 27 h of CSR, while mRNA levels of the pro-inflammatory cytokines TNFα, IL1β, and IL6 remained unchanged at 27 and 99 h of CSR. The latter finding may be explained by previous reports that IL10 can inhibit microglial production of TNFα, IL1β, and IL6 [73, 74]. Our findings, however, are in contrast to previously reported increases in TNFα and IL1β mRNA levels in the frontal cortex and hippocampus after 5 days of CSR [42], and in the piriform cortex and hippocampus after 21 days of CSR [75] in adult rats, as well as increases in TNFα and IL6 mRNA levels in the hippocampus after 72 h of REM sleep deprivation in adult mice [12, 76]. Nonetheless, mRNA levels do not necessarily predict protein levels, and several cytokine mRNAs are known to be post-transcriptionally modified [77]. Another study in adolescent mice found a decrease in TNFα protein levels, no change in IL1β protein levels, and undetectable IL6 and IL10 protein levels in the cerebrospinal fluid after 4.5 days of CSR [10]. The discrepancies among these studies are likely due to differences in species, duration of CSR, and/or protocol used, as well as samples (brain regions or cerebrospinal fluid), or mRNA or protein, that were analyzed. Finally, although microglia are one of the best characterized cellular sources of IL10 in the brain [78], in situ hybridization is necessary to confirm the cellular localization of IL10 mRNA.

The function of increased IL10 mRNA and possibly protein levels requires further investigation. We previously found that BDNF protein levels were increased in the frontal cortex following 27 h, with a slight decline in this increase after 99 h, of the 3/1 CSR protocol [19]. BDNF has been shown to increase the expression of IL10 in a rat model of ischemia [79]. Binding of IL10 at its receptor, present on both glial and neuronal cell types, promotes the survival of both glia and neurons [78]. Therefore, neuroprotective molecules such as IL10 and BDNF may interact to initiate processes that help animals adapt to CSR.

Homeostatic state of CSR-responsive microglia

Iba1 is involved in cytoskeletal reorganization and phagocytosis [80, 81], and Iba1 protein levels are upregulated in microglia in response to pathophysiological stimuli, in parallel with a withdrawal of processes and cell body enlargement plus an increased expression of inflammatory markers [82–85]. Thus, the increased Iba1 immunoreactivity observed in response to CSR could suggest an inflammatory response. However, several aspects of the microglia response to the 3/1 CSR protocol are not congruent with inflammatory activation [86]. First, microglia morphology was not affected by CSR and microglia remained ramified as confirmed quantitatively in the prefrontal cortex. Second, microglia in the frontal cortex did not contain pro-inflammatory (CD68 and OX6) or anti-inflammatory (arginase-1, cyclooxygenase-2, and mannose receptor) markers. Third, mRNA levels of several pro-inflammatory cytokines were not affected, although mRNA levels of the anti-inflammatory cytokine IL10 were transiently increased, in the frontal cortex by CSR. Fourth, despite the increased Iba1 density and/or numbers of Iba1-ir cells, there was no evidence of microglial proliferation or peripheral macrophage recruitment. Collectively, these results indicate that microglia do not respond to the 3/1 CSR protocol with inflammatory activation.

Consistent with the lack of inflammatory responses to the 3/1 protocol, we found that microglia in the frontal cortex contain the purinergic P2Y12 receptor. This $G_{i/o}$ protein-coupled

receptor is expressed in microglia under physiological conditions and is down-regulated during inflammatory responses [27, 69]. Increasing evidence suggests that the P2Y12 receptor in microglia is involved in detecting extracellular signals such as nucleotides to induce chemotaxis, and its expression is thought to indicate the physiological or homeostatic state of microglia [27, 46, 87]. Homeostatic microglia respond to neuronal activity [46, 88, 89] and glutamatergic and GABAergic transmission, via nucleotides and other mediators [90–92]. Thus, microglia may respond to the sustained activity of wake-active neurons and their synaptic activities during sleep deprivation periods of the 3/1 CSR protocol. We found increased Iba1 immunoreactivity in the perifornical lateral hypothalamic area and the dorsal raphe nucleus, both of which contain wake-active neurons [93, 94], and we previously found evidence for increased neuronal activation (indicated by increased ΔFosB/FosB immunoreactivity) in the perifornical lateral hypothalamic area using the same 3/1 CSR protocol [24]. In the present study, increased Iba1 immunoreactivity also occurred in the prelimbic cortex, which plays a role in sustained attention and working memory [95] and is thought to be particularly sensitive to sleep loss [41]. Homeostatic microglia can initiate synaptic plasticity by contacting spines [96] and phagocytosing pre-synaptic elements [97] through P2Y12 receptor activation [98]. Microglia phagocytosis of presynaptic terminals was reported in the adolescent mouse cortex after 4.5 h of CSR [10] (but see Ref. [99]), while impaired microglia phagocytosis of post-synaptic elements was associated with a reduction of P2Y12 receptor mRNA levels in the adolescent mouse hippocampus after 72 h of selective REM sleep deprivation [12]. These forms of synaptic plasticity, if they occur in the perifornical lateral hypothalamic area, dorsal raphe nucleus, and prelimbic cortex in response to CSR, might be involved in the adaptive changes in sleep/wake patterns and sustained attention observed during the 3/1 CSR protocol [17, 18].

Conclusions

Our data indicate that sleep-restricting rats for 1–4 days using the 3/1 CSR protocol resulted in time-dependent and region-specific increases in microglial Iba1 immunoreactivity in the brain. Microglia remained in a physiological state without inflammatory activation. The CSR-induced microglial responses in a subset of sleep/wake and limbic brain regions may be involved in adaptive changes in sleep homeostasis and sustained attention in response to chronic sleep loss. In addition, the microglial response to CSR could alter the way microglia react to subsequent challenges, thereby modifying brain vulnerability to damage by further insults. Whether the microglial response persists during recovery following CSR remains to be investigated.

Supplementary material

Supplementary material is available at *SLEEP* online.

Funding

This work was supported by the Canadian Institutes for Health Research [MOP-259183, PJT-159779], Dalhousie Medical Research Foundation, and Plum Foundation. Funding sources had no involvement in study design; in the collection, analysis, and interpretation of data; in the writing of the report; and in the decision to submit the article for publication.

Financial Disclosure: None.

Nonfinancial Disclosure: None.

Acknowledgments

We thank J. Burns for technical assistance in brain dissection and immunohistochemistry; S. Whitefield for technical support for microscopy and imaging; M. Wigerius for technical advice for Sholl analysis; N. Barthel for assistance in animal care and help with analysis of Evans Blue extravasation; K. Murphy and A. Friedman for helpful discussion of blood–brain barrier permeability methods; and A. Lammie and E. Belland for technical assistance with qRT-PCR.

Conflict of interest statement. None declared.

References

1. Aldabal L, *et al*. Metabolic, endocrine, and immune consequences of sleep deprivation. *Open Respir Med J*. 2011;**5**:31–43.
2. Banks S, *et al*. Behavioral and physiological consequences of sleep restriction. *J Clin Sleep Med*. 2007;**3**:519–528.
3. Ingiosi AM, *et al*. Sleep and immune function: glial contributions and consequences of aging. *Curr Opin Neurobiol*. 2013;**23**:806–811.
4. Zhao Z, *et al*. Neural consequences of chronic short sleep: reversible or lasting? *Front Neurol*. 2017;**8**:235.
5. Kim SU, *et al*. Microglia in health and disease. *J Neurosci Res*. 2005;**81**:302–313.
6. Streit WJ, *et al*. Microglia and neuroinflammation: a pathological perspective. *J Neuroinflammation*. 2004;**1**:14.
7. Delpech JC, *et al*. Microglia in neuronal plasticity: influence of stress. *Neuropharmacology*. 2015;**96**:19–28.
8. Kierdorf K, *et al*. Microglia in steady state. *J Clin Invest*. 2017;**127**:3201–3209.
9. Wisor JP, *et al*. Evidence for neuroinflammatory and microglial changes in the cerebral response to sleep loss. *Sleep*. 2011;**34**:261–272.
10. Bellesi M, *et al*. Sleep loss promotes astrocytic phagocytosis and microglial activation in mouse cerebral cortex. *J Neurosci*. 2017;**37**:5263–5273.
11. Hsu JC, *et al*. Sleep deprivation inhibits expression of NADPH-d and NOS while activating microglia and astroglia in the rat hippocampus. *Cells Tissues Organs*. 2003;**173**:242–254.
12. Tuan LH, *et al*. Microglia-mediated synaptic pruning is impaired in sleep-deprived adolescent mice. *Neurobiol Dis*. 2019;**130**:104517.
13. Wadhwa M, *et al*. Caffeine and modafinil ameliorate the neuroinflammation and anxious behavior in rats during sleep deprivation by inhibiting the microglia activation. *Front Cell Neurosci*. 2018;**12**:49.
14. Wadhwa M, *et al*. Sleep deprivation induces spatial memory impairment by altered hippocampus neuroinflammatory responses and glial cells activation in rats. *J Neuroimmunol*. 2017;**312**:38–48.
15. Zhu B, *et al*. Sleep disturbance induces neuroinflammation and impairment of learning and memory. *Neurobiol Dis*. 2012;**48**:348–355.
16. Xie Y, *et al*. Chronic sleep fragmentation shares similar pathogenesis with neurodegenerative diseases:

endosome-autophagosome-lysosome pathway dysfunction and microglia-mediated neuroinflammation. *CNS Neurosci Ther*. 2020;**26**:215–227.
17. Deurveilher S, *et al*. Time-of-day modulation of homeostatic and allostatic sleep responses to chronic sleep restriction in rats. *Am J Physiol Regul Integr Comp Physiol*. 2012;**302**:R1411–R1425.
18. Deurveilher S, *et al*. Psychomotor vigilance task performance during and following chronic sleep restriction in rats. *Sleep*. 2015;**38**:515–528.
19. Wallingford JK, *et al*. Increases in mature brain-derived neurotrophic factor protein in the frontal cortex and basal forebrain during chronic sleep restriction in rats: possible role in initiating allostatic adaptation. *Neuroscience*. 2014;**277**:174–183.
20. Huang EJ, *et al*. Neurotrophins: roles in neuronal development and function. *Annu Rev Neurosci*. 2001;**24**:677–736.
21. Chou TC, *et al*. Critical role of dorsomedial hypothalamic nucleus in a wide range of behavioral circadian rhythms. *J Neurosci*. 2003;**23**:10691–10702.
22. Faraguna U, *et al*. A causal role for brain-derived neurotrophic factor in the homeostatic regulation of sleep. *J Neurosci*. 2008;**28**:4088–4095.
23. Huber R, *et al*. Exploratory behavior, cortical BDNF expression, and sleep homeostasis. *Sleep*. 2007;**30**:129–139.
24. Hall S, *et al*. Region-specific increases in FosB/ΔFosB immunoreactivity in the rat brain in response to chronic sleep restriction. *Behav Brain Res*. 2017;**322**:9–17.
25. Chen J, *et al*. Chronic Fos-related antigens: stable variants of deltaFosB induced in brain by chronic treatments. *J Neurosci*. 1997;**17**:4933–4941.
26. Franco R, *et al*. Alternatively activated microglia and macrophages in the central nervous system. *Prog Neurobiol*. 2015;**131**:65–86.
27. Haynes SE, *et al*. The P2Y12 receptor regulates microglial activation by extracellular nucleotides. *Nat Neurosci*. 2006;**9**:1512–1519.
28. Mildner A, *et al*. P2Y12 receptor is expressed on human microglia under physiological conditions throughout development and is sensitive to neuroinflammatory diseases. *Glia*. 2017;**65**:375–387.
29. Deurveilher S, *et al*. Social and environmental contexts modulate sleep deprivation-induced c-Fos activation in rats. *Behav Brain Res*. 2013;**256**:238–249.
30. Scammell TE, *et al*. Neural circuitry of wakefulness and sleep. *Neuron*. 2017;**93**:747–765.
31. Bonde S, *et al*. Long-term neuronal replacement in adult rat hippocampus after status epilepticus despite chronic inflammation. *Eur J Neurosci*. 2006;**23**:965–974.
32. Junek A, *et al*. Short-term sleep deprivation may alter the dynamics of hippocampal cell proliferation in adult rats. *Neuroscience*. 2010;**170**:1140–1152.
33. Gómez-González B, *et al*. REM sleep loss and recovery regulates blood-brain barrier function. *Curr Neurovasc Res*. 2013;**10**:197–207.
34. Yen LF, *et al*. Distinct patterns of cerebral extravasation by Evans blue and sodium fluorescein in rats. *PLoS One*. 2013;**8**:e68595.
35. del Valle J, *et al*. A new method for determining blood-brain barrier integrity based on intracardiac perfusion of an Evans Blue-Hoechst cocktail. *J Neurosci Methods*. 2008;**174**:42–49.
36. Lee KS, *et al*. Validation of commonly used reference genes for sleep-related gene expression studies. *BMC Mol Biol*. 2009;**10**:45.
37. Nichols M, *et al*. Synergistic neuroprotection by epicatechin and quercetin: activation of convergent mitochondrial signaling pathways. *Neuroscience*. 2015;**308**:75–94.
38. Bustin SA, *et al*. The MIQE guidelines: minimum information for publication of quantitative real-time PCR experiments. *Clin Chem*. 2009;**55**:611–622.
39. Hinwood M, *et al*. Chronic stress induced remodeling of the prefrontal cortex: structural re-organization of microglia and the inhibitory effect of minocycline. *Cereb Cortex*. 2013;**23**:1784–1797.
40. Morrison HW, *et al*. A quantitative spatiotemporal analysis of microglia morphology during ischemic stroke and reperfusion. *J Neuroinflammation*. 2013;**10**:4.
41. Muzur A, *et al*. The prefrontal cortex in sleep. *Trends Cogn Sci*. 2002;**6**:475–481.
42. Zielinski MR, *et al*. Chronic sleep restriction elevates brain interleukin-1 beta and tumor necrosis factor-alpha and attenuates brain-derived neurotrophic factor expression. *Neurosci Lett*. 2014;**580**:27–31.
43. Karperien A, *et al*. Quantitating the subtleties of microglial morphology with fractal analysis. *Front Cell Neurosci*. 2013;**7**:3.
44. Hinwood M, *et al*. Evidence that microglia mediate the neurobiological effects of chronic psychological stress on the medial prefrontal cortex. *Cereb Cortex*. 2012;**22**:1442–1454.
45. Tynan RJ, *et al*. Chronic stress alters the density and morphology of microglia in a subset of stress-responsive brain regions. *Brain Behav Immun*. 2010;**24**:1058–1068.
46. Cserép C, *et al*. Microglia monitor and protect neuronal function through specialized somatic purinergic junctions. *Science*. 2020;**367**:528–537.
47. Chinnery HR, *et al*. Novel characterization of monocyte-derived cell populations in the meninges and choroid plexus and their rates of replenishment in bone marrow chimeric mice. *J Neuropathol Exp Neurol*. 2010;**69**:896–909.
48. Hellström Erkenstam N, *et al*. Temporal characterization of microglia/macrophage phenotypes in a mouse model of neonatal hypoxic-ischemic brain injury. *Front Cell Neurosci*. 2016;**10**:286.
49. Faraco G, *et al*. Brain perivascular macrophages: characterization and functional roles in health and disease. *J Mol Med (Berl)*. 2017;**95**:1143–1152.
50. Burudi EM, *et al*. Regional and cellular expression of the mannose receptor in the post-natal developing mouse brain. *Cell Tissue Res*. 2001;**303**:307–317.
51. Kaufmann WE, *et al*. COX-2, a synaptically induced enzyme, is expressed by excitatory neurons at postsynaptic sites in rat cerebral cortex. *Proc Natl Acad Sci U S A*. 1996;**93**:2317–2321.
52. Kuric E, *et al*. Dynamics of major histocompatibility complex class II-positive cells in the postischemic brain–influence of levodopa treatment. *J Neuroinflammation*. 2014;**11**:145.
53. Perego C, *et al*. Temporal pattern of expression and colocalization of microglia/macrophage phenotype markers following brain ischemic injury in mice. *J Neuroinflammation*. 2011;**8**:174.
54. Peters D, *et al*. Arginase and arginine decarboxylase—where do the putative gate keepers of polyamine synthesis reside in rat brain? *PLoS One*. 2013;**8**:e66735.
55. Barf RP, *et al*. Metabolic consequences of chronic sleep restriction in rats: changes in body weight regulation and energy expenditure. *Physiol Behav*. 2012;**107**:322–328.
56. Everson CA, *et al*. Repeated exposure to severely limited sleep results in distinctive and persistent physiological imbalances in rats. *PLoS One*. 2011;**6**:e22987.

57. Lovatel GA, *et al*. Long-term effects of pre and post-ischemic exercise following global cerebral ischemia on astrocyte and microglia functions in hippocampus from Wistar rats. *Brain Res*. 2014;**1587**:119–126.
58. Olah M, *et al*. Enhanced hippocampal neurogenesis in the absence of microglia T cell interaction and microglia activation in the murine running wheel model. *Glia*. 2009;**57**:1046–1061.
59. Chennaoui M, *et al*. Effects of exercise on brain and peripheral inflammatory biomarkers induced by total sleep deprivation in rats. *J Inflamm (Lond)*. 2015;**12**:56.
60. Meerlo P, *et al*. Sleep restriction alters the hypothalamic-pituitary-adrenal response to stress. *J Neuroendocrinol*. 2002;**14**:397–402.
61. Roman V, *et al*. Too little sleep gradually desensitizes the serotonin 1A receptor system. *Sleep*. 2005;**28**:1505–1510.
62. Wohleb ES, *et al*. Peripheral innate immune challenge exaggerated microglia activation, increased the number of inflammatory CNS macrophages, and prolonged social withdrawal in socially defeated mice. *Psychoneuroendocrinology*. 2012;**37**:1491–1505.
63. Bennett ML, *et al*. New tools for studying microglia in the mouse and human CNS. *Proc Natl Acad Sci U S A*. 2016;**113**:E1738–E1746.
64. Roy A, *et al*. Up-regulation of microglial CD11b expression by nitric oxide. *J Biol Chem*. 2006;**281**:14971–14980.
65. Streit WJ, *et al*. Reactive microgliosis. *Prog Neurobiol*. 1999;**57**:563–581.
66. Banasr M, *et al*. Chronic unpredictable stress decreases cell proliferation in the cerebral cortex of the adult rat. *Biol Psychiatry*. 2007;**62**:496–504.
67. He J, *et al*. Sleep restriction impairs blood-brain barrier function. *J Neurosci*. 2014;**34**:14697–14706.
68. Hurtado-Alvarado G, *et al*. Chronic sleep restriction disrupts interendothelial junctions in the hippocampus and increases blood-brain barrier permeability. *J Microsc*. 2017;**268**:28–38.
69. Amadio S, *et al*. P2Y(12) receptor on the verge of a neuroinflammatory breakdown. *Mediators Inflamm*. 2014;**2014**:975849.
70. Butovsky O, *et al*. Identification of a unique TGF-β-dependent molecular and functional signature in microglia. *Nat Neurosci*. 2014;**17**:131–143.
71. Nimmerjahn A, *et al*. Resting microglial cells are highly dynamic surveillants of brain parenchyma in vivo. *Science*. 2005;**308**:1314–1318.
72. Wake H, *et al*. Microglia: actively surveying and shaping neuronal circuit structure and function. *Trends Neurosci*. 2013;**36**:209–217.
73. Lodge PA, *et al*. Regulation of microglial activation by TGF-beta, IL-10, and CSF-1. *J Leukoc Biol*. 1996;**60**:502–508.
74. Sawada M, *et al*. Interleukin-10 inhibits both production of cytokines and expression of cytokine receptors in microglia. *J Neurochem*. 1999;**72**:1466–1471.
75. Manchanda S, *et al*. Low-grade neuroinflammation due to chronic sleep deprivation results in anxiety and learning and memory impairments. *Mol Cell Biochem*. 2018;**449**:63–72.
76. Xue R, *et al*. Nicotinic mitigation of neuroinflammation and oxidative stress after chronic sleep deprivation. *Front Immunol*. 2019;**10**:2546.
77. Vlasova-St Louis I, *et al*. Post-transcriptional regulation of cytokine and growth factor signaling in cancer. *Cytokine Growth Factor Rev*. 2017;**33**:83–93.
78. Lobo-Silva D, *et al*. Balancing the immune response in the brain: IL-10 and its regulation. *J Neuroinflammation*. 2016;**13**:297.
79. Jiang Y, *et al*. Intranasal brain-derived neurotrophic factor protects brain from ischemic insult via modulating local inflammation in rats. *Neuroscience*. 2011;**172**:398–405.
80. Imai Y, *et al*. Intracellular signaling in M-CSF-induced microglia activation: role of Iba1. *Glia*. 2002;**40**:164–174.
81. Sasaki Y, *et al*. Iba1 is an actin-cross-linking protein in macrophages/microglia. *Biochem Biophys Res Commun*. 2001;**286**:292–297.
82. Ito D, *et al*. Microglia-specific localisation of a novel calcium binding protein, Iba1. *Brain Res Mol Brain Res*. 1998;**57**:1–9.
83. Ito D, *et al*. Enhanced expression of Iba1, ionized calcium-binding adapter molecule 1, after transient focal cerebral ischemia in rat brain. *Stroke*. 2001;**32**:1208–1215.
84. Leasure JL, *et al*. Forced and voluntary exercise differentially affect brain and behavior. *Neuroscience*. 2008;**156**:456–465.
85. Orihuela R, *et al*. Microglial M1/M2 polarization and metabolic states. *Br J Pharmacol*. 2016;**173**:649–665.
86. Perry VH, *et al*. Microglia in neurodegenerative disease. *Nat Rev Neurol*. 2010;**6**:193–201.
87. Calovi S, *et al*. Microglia and the purinergic signaling system. *Neuroscience*. 2019;**405**:137–147.
88. Wake H, *et al*. Resting microglia directly monitor the functional state of synapses in vivo and determine the fate of ischemic terminals. *J Neurosci*. 2009;**29**:3974–3980.
89. Tremblay MÈ, *et al*. Microglial interactions with synapses are modulated by visual experience. *PLoS Biol*. 2010;**8**:e1000527.
90. Fontainhas AM, *et al*. Microglial morphology and dynamic behavior is regulated by ionotropic glutamatergic and GABAergic neurotransmission. *PLoS One*. 2011;**6**:e15973.
91. Dissing-Olesen L, *et al*. Activation of neuronal NMDA receptors triggers transient ATP-mediated microglial process outgrowth. *J Neurosci*. 2014;**34**:10511–10527.
92. Bernier LP, *et al*. Nanoscale surveillance of the Brain by Microglia via cAMP-regulated Filopodia. *Cell Rep*. 2019;**27**:2895–2908.e4.
93. Fuller PM, *et al*. Neurobiology of the sleep-wake cycle: sleep architecture, circadian regulation, and regulatory feedback. *J Biol Rhythms*. 2006;**21**:482–493.
94. Hassani OK, *et al*. Melanin-concentrating hormone neurons discharge in a reciprocal manner to orexin neurons across the sleep-wake cycle. *Proc Natl Acad Sci U S A*. 2009;**106**:2418–2422.
95. Granon S, *et al*. Involvement of the rat prefrontal cortex in cognitive functions: a central role for the prelimbic area. *Psychobiology*. 2000;**28**:229–237.
96. Akiyoshi R, *et al*. Microglia enhance synapse activity to promote local network synchronization. *eNeuro*. 2018;**5**:ENEURO.0088-18.
97. Schafer DP, *et al*. Microglia sculpt postnatal neural circuits in an activity and complement-dependent manner. *Neuron*. 2012;**74**:691–705.
98. Sipe GO, *et al*. Microglial P2Y12 is necessary for synaptic plasticity in mouse visual cortex. *Nat Commun*. 2016;**7**:10905.
99. Choudhury ME, *et al*. Phagocytic elimination of synapses by microglia during sleep. *Glia*. 2020;**68**:44–59.